Pinning-induced pn junction formation in low-bandgap two-dimensional semiconducting systems

David A. Deen^{1, a)}

independent submission

A model is presented for pn junction formation near metal-semiconductor contacts in two-dimensional semiconducting systems such as graphene. Carrier type switching occurs in a region near the metal-semiconductor junction when energy band bending leads to a crossing between the junction Fermi level and the Dirac energy. A bias-dependent depletion region occurs due to the minimization of carrier density, which is shown to act as an additional parasitic resistance in devices. The pn junction resistance is demonstrated by its implementation in a transfer length structure.

a) Electronic mail: david.deen@alumni.nd.edu

The advent of two-dimensional (2D) semiconducting systems, such as graphene and the transition-metal dichalcogenides, has driven significant efforts to utilize these systems for electronic devices.^{1,2} In the vast majority of embodiments, electronic devices like the field effect transistor and various sensor designs utilize a modulated channel.³ In those cases, metallic electrodes are used to make ohmic contact to the semiconducting channel. Most studies address the minimization of parasitic access resistance via the contact resistance (R_c) of the contacts to graphene. 4-6 However, little attention has been given to the manifestation of spuriously high-resistance pn junctions formed in close proximity to the contact. The formation of the pn junction is due to the contrast between the Fermi-energy pinning at the metal-semiconductor interface and opposite carrier typing outside the contact region that results from ambient electrostatic bias. Ultimately, the pn junction resistance results as an additive parasitic resistance to the other parasitic resistances (access, R_{acc} , and R_c) present, which may subsequently serve to impair device performance. This work presents the development of an electrostatic model that describes the formation of such a pn junction with low carrier density in proximity to a metal-2D semiconductor contact. The energy intersection between the pinned Fermi level under the metal-semiconductor contact and the 2D semiconductor Dirac energy (E_D) is central to the development and results in the low carrier density bias-dependent pn junction. The model includes calculations for the width of minimum conductivity, its dependence on voltage bias, and how it is manifested in a conventional test structure. More complex effects such as Klein tunneling and the role of band chirality on carrier generation-recombination are not incorporated in the electrostatic model but likely play a role in the transport picture.⁷

Graphene and some transition-metal dichalcogenide semiconductors exhibit a unique linear energy dispersion relation due to hybridized sp² covalent bonding within their bravais lattice. In this work zero-bandgap graphene is used as an example from the broad 2D semiconducting families. Figure 1 shows an illustration of a graphene device cross-section near one ohmic contact (a) with the linearized energy band diagram (b) and resultant total charge distribution (c) for several voltage biases. The ohmic contact was assumed to pin the graphene Fermi level at an energy of η_p only under the contact.^{4,5,8} The linearization of the energy band diagram is an approximation made only in a small energy range about the Fermi level-Dirac energy (F-D) intersection where total charge density is minimized and resistance has a maximum. Realistically, the Dirac energy (or conduction and valence band

intersection) bends throughout the length of the device in the x-direction in coherence with a change in charge density (Poisson). However, for the small energy range about the F-D crossing the linearized energy is sufficient to describe the carrier typing and therefore, the electrostatics of the system in the vicinity of the ohmic contact.

An approximation has been made for the resistance associated with the region beyond the linear energy region where $|(E_D - E_f)| \gg |\eta_p|$. In this region, the total charge density exponentially increases according to Fermi-Dirac statistics and yields a resistance much less than in the region where the F-D crossing occurs. Therefore, this low-resistance extension has been treated as the sheet resistance outside the proximity of the F-D intersection (regions beyond W_d in Fig. 1 (c)). The pinning energy polarity at the metal-graphene junction and the ambient electrostatic bias away from the contact are responsible for setting up the conditions leading to the F-D intersection and therefore, the attributes of the pn junction. Those conditions determined the polarity of the E_D slope, number of F-D intersection within a given region, and length of total charge minimum referred to as the 'depletion width' (W_d) in this work. If two F-D intersections occur, the total resistance becomes approximately twice the resistance of a single pn junction.

The carrier distribution in graphene results from the linear dispersion relation and therefore follows from the full Fermi-Dirac integral, $n, p(\eta) = qN_G\mathcal{F}_i(\pm\eta)$ where $\mathcal{F}_i(\pm\eta) = (\Gamma(i+1))^{-1} \int_0^\infty u^i (1+e^{\mp\eta}e^u)^{-1} du$.^{3,9} The longitudinally-dependent total charge is given as

$$Q_{tot}(x) = \frac{qN_G}{\Gamma(2)} \left[\int_0^\infty \frac{udu}{1 + e^u e^{\phi_F(x)}} - \int_0^\infty \frac{udu}{1 + e^u e^{-\phi_F(x)}} \right]$$
(1)

where $N_G = (g_s g_v/2\pi)(k_B T/\hbar v_F)^2$ is the 2D density of states with g_s and g_v are the spin and valley degeneracies, respectively, v_F is the Fermi velocity, q the elemental charge, $\Gamma(\dots)$ is the gamma function, \hbar is the reduced Planck's constant, $\phi_F(x) = k_B T \eta_F(x)$ is the energy along the channel normalized by the thermal energy $k_B T$, k_B is Boltzmann's constant, and T the temperature. The linearized energy band was approximated as, $E - E_f = V_a(x - x_o)/L$, where x_o is at the ohmic contact edge as illustrated in Fig. 1. The normalized longitudinal energy term used in Eq. 1 follows from the boundary conditions of the linear energy band,

$$\eta_F(x) = \frac{qV_a}{L}x - \eta_p \tag{2}$$

where L is the length of the graphene sheet between the two biased contacts as defined in

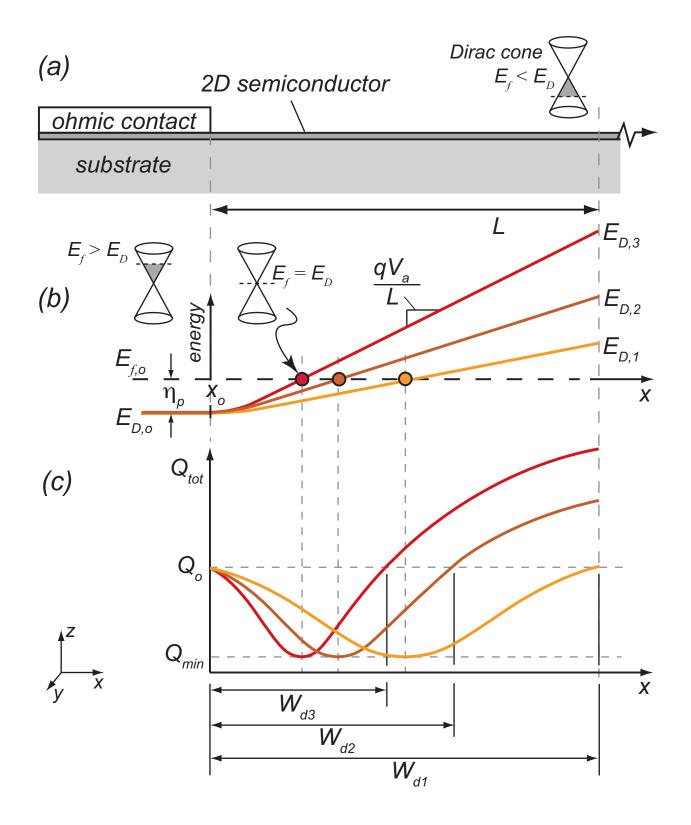


FIG. 1. (a) Illustration of the 2D structure, (b) lateral band diagram in graphene along the sourcedrain direction at several different voltage biases, and (c) the resultant carrier density profiles along the graphene channel.

Fig. 1, V_a is the applied voltage, and η_p is the contact pinning energy. The depletion width is defined as twice the distance from contact pinning to the Fermi level crossing and follows

$$W_d = \frac{2\eta_p L}{qV_a} \tag{3}$$

In the conventional case of a three-dimensional semiconductor pn junction, the depletion width is defined by the balance of the internal field and the diffusion of free carriers. The linear energy approximation accounts for the complete electrostatic picture for the pinning-induced pn junction in graphene. The total resistance of the depletion width accounting for the single Fermi level crossing, is given by the integral relationship,

$$R_d = \frac{1}{W_g} \int_0^{W_d} \frac{dx}{\sigma(x)} = \frac{1}{qW_g} \int_0^{W_d} \frac{dx}{\mu_n n(x) + \mu_p p(x)}$$
(4)

where $\sigma(x) = q(\mu_n n(x) + \mu_p p(x))$ is the graphene conductivity and is dependent on the areal charge densities, n and p, and the respective carrier mobilities, μ_n and μ_p , and W_g is the cross-sectional width of the graphene sheet.

Parametric calculations are shown in Fig. 2 wherein Figs. 2 (a) and (c) show total charge density and correspondent resistivity ($\rho(x) = 1/\sigma(x)$) in the graphene sheet, respectively, as a function of distance away from the ohmic contact for several longitudinal voltages. A pinning energy of 4 eV has been used, which is commensurate with values reported.⁴⁻⁶ The charge density and resistivity minima progressively decreased with an increase in applied voltage as the F-D intersection migrated toward the ohmic contact. The rapidly diminished value of ρ away from the F-D crossing (total charge minima) validates the previously stated approximation. Figure 2 (b) and (d) show depletion width and depletion region resistance in the graphene sheet, respectively, as a function of applied voltage for several values of pinning energy. As a greater bias voltage is applied, energy-band bending is enhanced and the slope of the linear region becomes greater leading to the trends shown in Fig. 2. The bias-dependence of R_d is of note within the context that parasitic resistances are typically fixed (e.g. R_c or R_{acc}). A dynamic parasitic resistance like R_d may serve to complicate the extraction of other intrinsic device metrics (i.e. transistor transconductance, frequency performance, etc.). One method that may prove to disable the formation of the pn junction is doping graphene. By doping, the Fermi level in graphene can be significantly shifted such that no F-D intersection may occur. Both W_d and R_d linearly decreased with increasing voltage following Eq. 3 and 4, respectively.

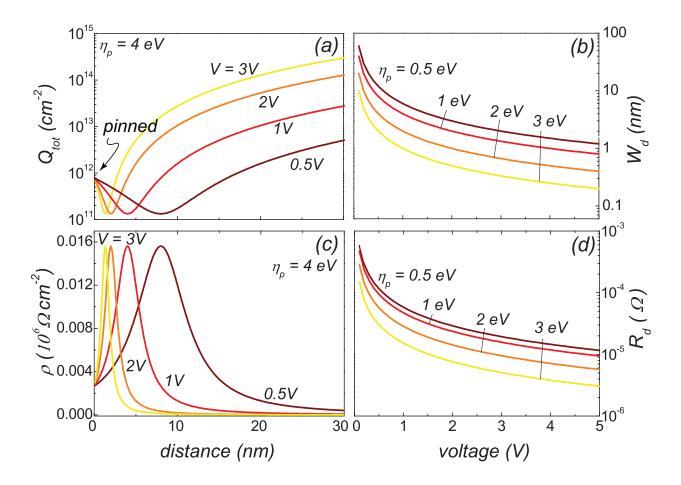


FIG. 2. Parametric characteristics for the pn junctions formed in graphene in proximity to an ohmic contact; (a) Charge density versus longitudinal distance, (b) resistivity versus distance for various applied voltages, (c) depletion width versus applied longitudinal voltage, and (d) depletion region resistance versus applied voltage for various pinning values.

The effect of the pn junction on a device is illustrated through implementation into a transfer length structure (TLM). The TLM structure is a conventional test structure to extract information on R_c and R_{sh} . The total resistance of a TLM structure is conventionally given by $R(L) = 2R_c + \frac{L}{W}R_{sh}$, where R_{sh} is the sheet resistance. For the scenario considered here, we assume there is a single pn junction between TLM contacts and the depletion width is small compared to the separation between contacts, $W_d \ll L$. The latter assumption is verified by the calculation of W_d as shown in Fig. 2(b). These assumptions result in the TLM resistance relationship for graphene,

$$R_{TLM} = 2R_c + R_d + R_{sh} \left(\frac{L - a}{W_g}\right) \tag{5}$$

with R_d being the depletion region resistance as given by Eq. 4 and a is the distance between

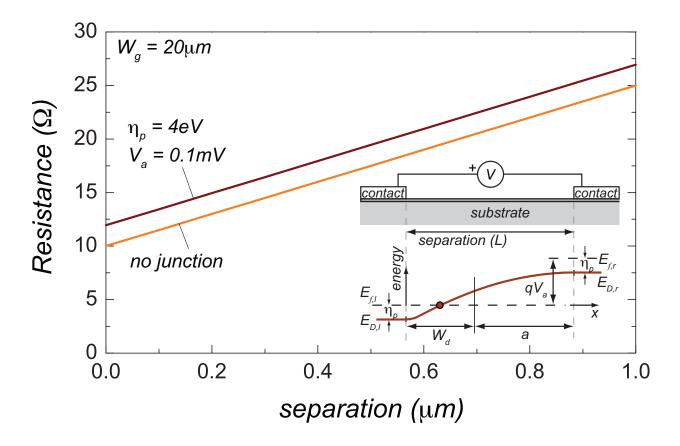


FIG. 3. Resistance of TLM structure comprised by graphene with and without the inclusion of a single pn junction showing a corresponding resistance increase. The inset shows the graphene TLM configuration and 1D linearized energy band diagram between two contacts.

the contacts and the depletion width as illustrated in the inset in Fig. 3. Written in terms of the longitudinal graphene conductivity and invoking the constraint, $L \gg a$, the total resistance of a graphene TLM structure with a single pn junction follows,

$$R(L) = 2R_c + \frac{L}{W_g} R_{sh} + \underbrace{\frac{1}{W_g} \int_{0}^{W_d} \frac{dx}{\sigma(x)}}_{R_d}$$

$$\tag{6}$$

Equation 6 shows that the presence of a single pn junction in the graphene sheet adds a resistance proportional to the total bias-dependent resistivity of the junction to the TLM resistance. The pn junction resistance is independent of separation, L, and therefore is additive. The manifestation of additional pn junction resistance is demonstrated in Fig. 3 where a single pn junction is included in a TLM resistance curve with a Fermi pinning of 4 eV compared to a curve that does not include a pinning-induced pn junction. Other pertinent

graphene parameters used in the calculation are $W_g = 20 \ \mu m$, $R_{sh} = 300 \ \Omega/\Box$, $\mu_n = \mu_p = 1000 \ cm^2/Vs$, T = 300 K, and $v_F = 1.1 \times 10^6 \ cm/s$. The linear energy approximation should hold for other 2D low bandgap semiconductors.

An electrostatic model has been presented for pn junction formation in graphene in close proximity to ohmic contacts where Fermi level pinning occurs. It has been shown that electrostatic depletion of charge within the pn junction introduces a bias-dependent high-resistance region. The effect of pinning-induced pn junction formation in graphene has been illustrated for the case of a TLM structure, wherein the junction resistance was shown to be an additive term to the total TLM resistance. The broader impact of pn junction formation in low-bandgap two-dimensional systems may be spurious resistance that impairs device performance.

We would like to thank J. G. Champlain at the Naval Research Laboratory for helpful technical discussion.

REFERENCES

¹Novoselov, K. S., Geim, A. K., Morozov, S. V., Jiang, D., Katsnelson, M. I., Grigorieva, I. V., Dubonos, S. V., Firsov, A. A.: 'Two-dimensional gas of massless Dirac fermions in graphene', *Nature*, 2005, **438**, p. 197

²Radisavljevic, B., Radenovic, A., Brivio, J., Giacometti, V., Kis, A., 'Single-layer MoS₂ transistors', *Nat. Nanotech.*, 2011, **6**, p. 147

³Champlain, J.G.: 'A first principles theoretical examination of graphene-based field effect transistors', J. Appl. Phys., 2011, **109**, p. 084515

⁴Chaves, F. A., Jimenez, D., Cummings, A. W., Roch, S.: 'Physical model of the contact resistivity of metal-graphene junctions', *J. Appl. Phys.*, 2014, **115**, p. 164513

⁵Robinson, J. A., LaBella, M., Zhu, M., Hollander M., Kasarda R., Hughes, Z., Trumbull K., Cavalero R., Snyder D., 'Contacting graphene', *Appl. Phys. Lett.*, 2011, **98**, p. 053103 ⁶Moon, J. S., Antcliffe M., Seo H. C., Curtis D., Lin S., Schmitz A., Milosavljevic I., Kiselev A. A., Ross R. S., Gaskill D. K., Campbell P. M., Fitch R. C., Lee K.-M., Asbeck P., 'Ultra-low resistance ohmic contacts in graphene field effect transistors', *Appl. Phys. Lett.*, 2012, **100**, p. 203512

⁷Katsnelson, M. I., Novoselov, K. S., Geim, A. K., 'Chiral tunneling and the Klein paradox

in graphene', Nat. Phys., 2006, 2, p. 620

⁸Giovannetti G., Khomyakov P. A., Brocks G., Karpan V. M., van den Brink J., Kelly P. J., 'Doping Graphene with Metal Contacts', *Phys. Rev. Lett.*, 2008, **101**, p. 026803

⁹Fang, T., Konar, A., Xing, H., Jena, D., 'Graphene statistics and quantum capacitance of graphene sheets and ribbons', *Appl. Phys. Lett.*, 2007, **91**, p. 092109